

Heat and Fluid Flow Analysis over Different Tube Inserts of Recuperator

TA-SUNG HUANG*, PAI-HSIANG WANG*, YU-WEI CHIU** and JIIN-YUH JANG**

**New Materials Research and Development Department
China Steel Corporation*

Hsiao Kang, Kaohsiung 81233, Taiwan, R.O.C.

***Department of Mechanical Engineering
National Cheng Kung University
Tainan, Taiwan, R.O.C.*

The thermal-hydraulic characteristics of both the inside of and the outside of tube banks of a recuperator are discussed in this study. The radiation effect was considered between the tube wall and the working fluid to evaluate the tube exterior performance. For the tube interior, the heat transfer and pressure drop data for turbulent flow are discussed for different kinds of tube inserts, including longitudinal strip inserts with/without holes and twisted-tape inserts with three different twist angles ($\alpha=15.3^\circ$, 24.4° and 34.3°). From the simulation results, it is found that the heat transfer coefficient and pressure drop of tube banks with strip inserts are 5–16% and 90–140% higher than those of tube banks without inserts. When strip inserts with holes are used, the heat transfer coefficient and pressure drop are 12–27% and 220–250% higher than those for tube banks without inserts. The heat transfer coefficient and pressure drop of tube banks with twisted-tape inserts of $\alpha=15.3^\circ$, 24.4° and 34.3° are, respectively, 6–32% & 130–170%, 12–43% & 240–280%, and 25–61% & 290–330% higher than those of tube banks without inserts. The numerical results of heat transfer coefficient for strip inserts without/with holes and twisted-tape inserts agreed with the experimental data within 4.1%, 4.5% and 8.5%, respectively.

1. INTRODUCTION

The efficient utilization, conversion and recovery of heat are the predominant engineering problems of the process industry. The plate-finned-tube heat exchanger is one of the most commonly used compact heat exchangers in automobiles, air-conditioners and chemical industries. The recuperator is a special purpose heat exchanger utilized to recycle the exhaust gas heat energy escaping from the furnace.

There are three different approaches for the enhancement of tube-side convective heat transfer: namely, insert devices, internal fins and integral roughness. Insert devices involve various geometric forms that are inserted in a smooth, circular tube. Internal fins and integral roughness require deformation of the material on the inside surface of a long tube. The method of preference depends on two factors: the performance and the initial cost.

For displaced enhancement devices, Koch⁽¹⁾ and Evans & Churchill⁽²⁾ tested two types of displaced insert devices, spaced disks and spaced streamline shapes, in laminar and turbulent flow. These two types of in-

sert had a substantially higher pressure drop than that for the twisted-tape inserts or the wire coil inserts. Tomas⁽³⁾ tested displaced wires for turbulent flow of water in an annulus. When the wires were axially spaced in pairs, separated approximately by nine wires diameters, the most favorable 'St/f' (St is Stanton number, f is friction factor) performance was obtained. Xie et al.⁽⁴⁾ provided the data on the louvered inserts for an oil ($Pr=41$, Pr is Prandtl number) in an electrically heated tube. The strips, with an approximately 45-degree angle and spaced at a distance P, were bent in alternate directions.

In wire coil inserts, the inserts are made by tightly wrapping a coil of spring wire on a circular rod. The wire coil inserts provide heat transfer enhancement by flow separation at the wire causing a fluid mixing in the downstream from a wall layer. The local heat transfer coefficient downstream from a wall attached wire has been reported on by Emerson.⁽⁵⁾ These studies suggest an approximate rule for picking the maximum effective wire size.

In extended surface inserts, the inserted device is formed as an aluminum extrusion. The aluminum extrusion is normally formed with five legs, although the

number of legs is a design choice and may be between four and eight. Hilding and Coogan⁽⁶⁾ provided the Colburn factor (j) and the friction factor (f) versus the Reynolds number (Re) data for a six-legged straight extrusion in turbulent flow. Trupp and Lau⁽⁷⁾ predicted the Nusselt number (Nu) and f for laminar flow in a tube having full height fins and with an angle between the fin legs that varied from 8 to 180 degrees. Date and Singham⁽⁸⁾ and Date⁽⁹⁾ first reported the numerical predictions of heat transfer and friction performance for fully developed flows in tube-side with twisted-tape inserts under the uniform heat flux (UHF) boundary condition. Marner and Bergles⁽¹⁰⁾ published the heat transfer and isothermal pressure drop data for the laminar flow of a viscous liquid, Polybulene 20, in circular tubes with twisted-tape inserts. The heating and cooling data were obtained in the deep laminar region (Reynolds number from 15 to 575) and the heat transfer enhancement in Nusselt number (Nu) was about 50 to 125 percent higher than the tubes without any inserts. Smithberg and Landis⁽¹¹⁾ developed a semi-empirical model for the friction factor and showed that the model properly predicted the data for tapes having the twist ratio (y) from 3.62 to ∞. Thorsen and Landis⁽¹²⁾ showed that centrifugal force provides an enhancement of heat transfer because it can mix the working fluid from the core region with the working fluid near the wall. Thorsen and Landis also developed the first semi-analytical model for turbulent heat transfer with a twisted-tape tube insert and indicated that the buoyancy effect arising from the density variations in the centrifugal field has an effect on heat transfer. The correlation of the Nusselt number for heating process and cooling process were also obtained in the study. Lopina and Bergles⁽¹³⁾ created a superposition model to account for the increased speed of the flow causing by the spiral flow and the centrifugal buoyancy effects in the tubes. Manglik and Bergles⁽¹⁴⁾ provided a correlation of the heat transfer coefficient based on the asymptotic method, and is valid for a constant wall temperature (T_w) and constant Heat flux (q) with Re_d > 10,000. The correlation is shown as $Nu_d / Nu_{d,y=\infty} = 1 + \left(\frac{0.769}{y} \right)$, where Nu_d is for a twisted-tape inserts and Nu_{d,y=∞} is for a tape having no twist.

From the literature review, there are few related three-dimensional numerical analyses for the tube inserts. In this study, a three-dimensional numerical analysis with different types of tube inserts is performed and compared. In order to calculate the heat transfer enhancement and the correlated pressure drop, a flat-plane with holes and a twisted-tape with three different twist angles (α = 15.3°, 24.4° and 34.3°) were tested as tube inserts in this study.

2. EXPERIMENTAL METHOD

2.1 Mathematical Analysis

Figure 1 presents the physical model and relevant geometrical dimensions in both numerical and experimental studies for the tubes and inserts. Three different kinds of tube insert were investigated in this study to compare the heat transfer enhancement with the bare tubes. Figure 2 shows the details of the numerical models used in this study. The working fluid is considered to be incompressible with constant properties and the flow is assumed to be turbulent, steady and to have no viscous dissipation. Heat radiation and dissipation between the tube surface and the working fluid were considered owing to the high temperature of the working fluid. For the turbulence calculation, the intensity of the turbulence at the inlet was set to be 3%. The three-dimensional equations of continuity, momentum, energy, turbulent kinetic energy, k, and the dissipation rate, ε, in the fluid region can be expressed as follows:

$$\frac{\partial \bar{u}_i}{\partial x_i} = 0 \dots\dots\dots(1)$$

$$\frac{\partial}{\partial x_i} \rho(\bar{u}_i \bar{u}_j) = -\frac{\partial \bar{p}}{\partial x_i} + \frac{\partial}{\partial x_i} \left[\mu_{eff} \left(\frac{\partial \bar{u}_i}{\partial x_j} + \frac{\partial \bar{u}_j}{\partial x_i} \right) - \rho \bar{u}_i' \bar{u}_j' \right] \dots\dots\dots(2)$$

$$\frac{\partial}{\partial x_j} \rho c_p (\bar{u}_j \bar{T}) = \bar{u}_j \frac{\partial \bar{p}}{\partial x_j} + \bar{u}_j' \frac{\partial \bar{p}'}{\partial x_j} + \frac{\partial}{\partial x_j} \left(k \frac{\partial \bar{T}}{\partial x_j} - \rho c_p \bar{u}_j' \bar{T}' \right) \dots\dots\dots(3)$$

$$\frac{\partial}{\partial x_i} (\rho \bar{u}_i k) = -\frac{\partial}{\partial x_i} \left(\frac{\mu_{eff}}{\sigma_k} \frac{\partial k}{\partial x_i} \right) + \rho (P_r - \epsilon) \dots\dots\dots(4)$$

$$\frac{\partial}{\partial x_i} (\rho \bar{u}_i \epsilon) = -\frac{\partial}{\partial x_i} \left(\frac{\mu_{eff}}{\sigma_\epsilon} \frac{\partial \epsilon}{\partial x_i} \right) + \rho \frac{\epsilon}{k} \left[\left(c_1 + c_3 \frac{P_r}{\epsilon} \right) P_r - c_2 \epsilon \right] \dots\dots\dots(5)$$

Equation (2) contains Reynolds stresses expressed using the extended *k-ε* turbulence model proposed by Wang and Chen.⁽¹⁵⁾

In order to consider the radiation effect, the Discrete-Ordinate Method⁽¹⁶⁾ was applied and the governing equation is introduced below:

$$(\Omega \cdot \Delta) I(r, \Omega) = -(\kappa + \zeta) I(r, \Omega) + \kappa I_b(r) + \frac{\zeta}{4\pi} \int_{4\pi} I(r, \Omega') \Phi(\Omega' \rightarrow \Omega) d\Omega' \dots\dots(6)$$

where *I*(*r*, Ω) is the radiation intensity, *I_b*(*r*) is the blackbody radiation intensity, and *k* and ζ are the absorption and scattering coefficients of the medium,

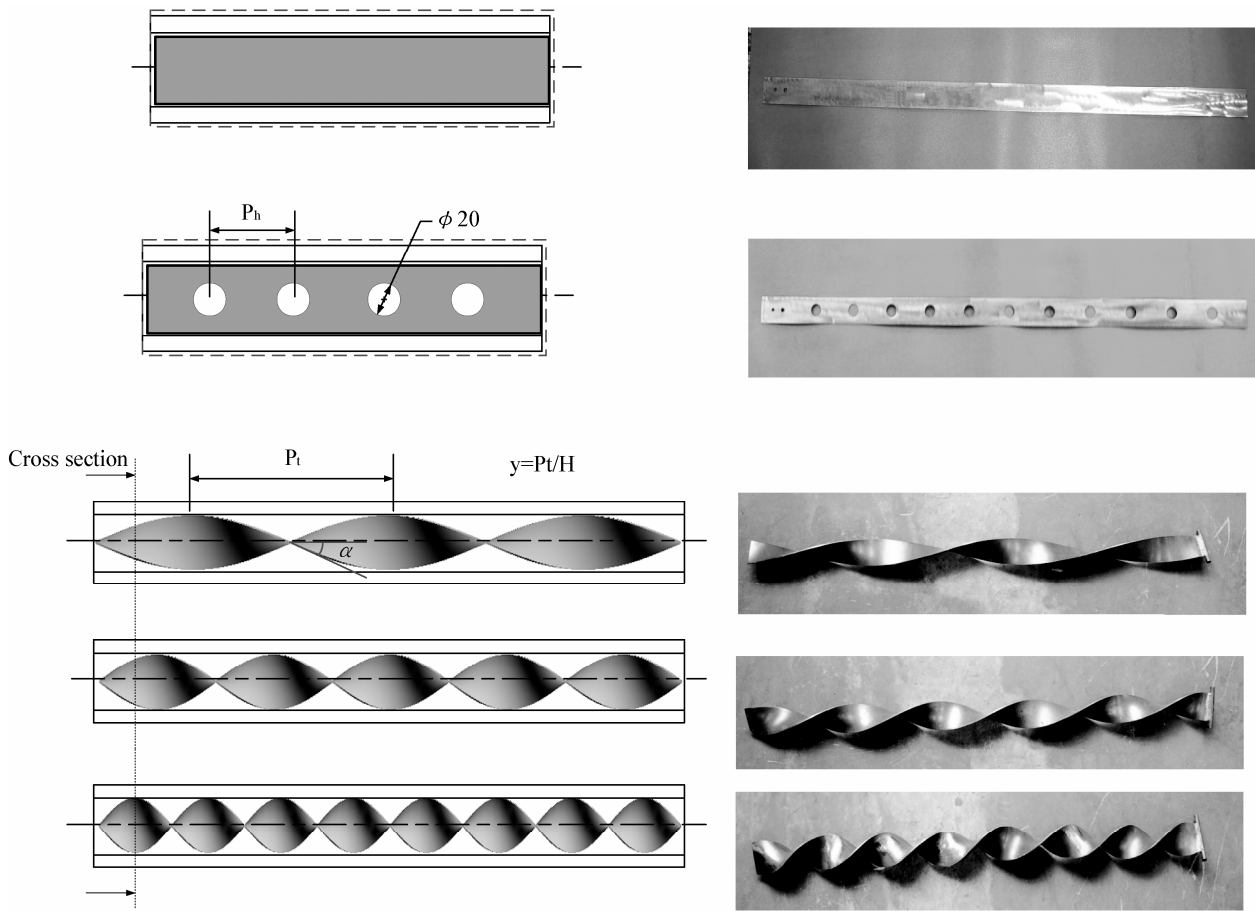


Fig. 1. Physical model of different tube inserts.

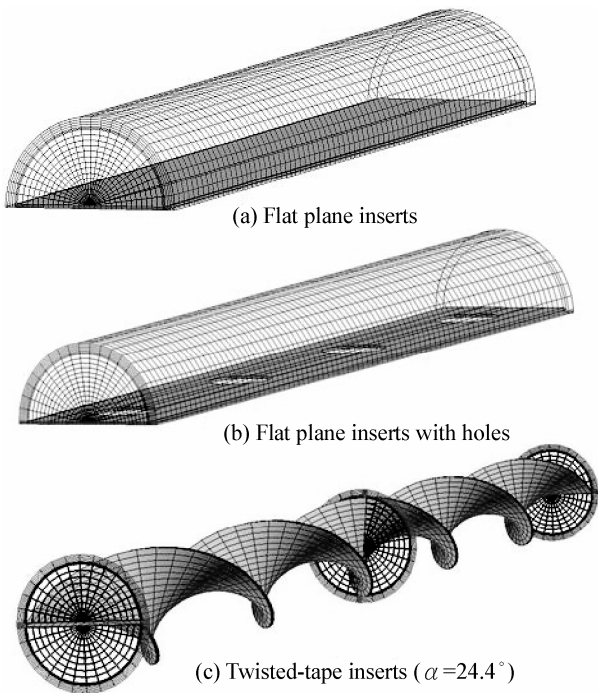


Fig. 2. Numerical models for tube inserts.

respectively. $\Phi(\Omega' \rightarrow \Omega)$ is the phase function of energy transfer from the incoming direction Ω' to the outgoing direction Ω . The left-hand side of Equation (6) represents the gradient of the intensity in the specified direction Ω . The three terms on the right-hand side represent the changes in the intensity due to the absorption and out scattering, emission, and the in scattering.

To obtain an accurate solution, proper boundary conditions have been applied on the boundary of the computational domain. At the upstream boundary, a uniform flow with the inlet velocity (U_{in}) and the inlet temperature (T_{in}) were assumed. At the downstream end of the computational domain, the stream-wise gradient (Neumann boundary conditions) for all the variables was set to be zero. At the symmetry planes, normal velocity was also set to be zero. At the solid surface, a no slip condition and a constant wall temperature (T_w) are specified.

A body-fitted coordinate system along a multiblock system is used in this study in order to generate a curvilinear coordinate system with a proper control of grid densities. The governing equations are solved numerically by using a control-volume-based finite-difference

formulation. The SIMPLER algorithm is used to solve the system of finite-difference equations iteratively. To fit the different types of tube inserts, axial-symmetry grids for bare tubes and biradial-symmetry grids for the flat-plane inserts, with and without holes, and twisted-tape tube inserts are used in this study.

2.2 Experimental Setup and Data Acquisition

The three types of tube insert configurations, namely flat-plane inserts, flat-plane inserts with holes and twisted-tape inserts with three different twist angles ($\alpha = 15.3^\circ$, 24.4° and 34.3°), tested in this study are shown in Fig. 1. Geometric parameters of all the tube inserts are also listed in Fig. 1. The experiments were conducted in an induced draft air system, as shown in Fig. 3. The hot air was driven by a 0.75 KW centrifugal fan and heated from room temperature to $300\text{--}700^\circ\text{C}$ by an electronic heater. The inlet and exit temperature across the test section were measured by a K-type thermocouple. The variation of these thermocouples was within $\pm 0.2^\circ\text{C}$ and the thermocouples were pre-calibrated by a quart thermometer whose accuracy is within 0.01°C . The working fluid inside the tube was cold air and both the inlet and the outlet temperatures were measured by two pre-calibrated RTDs (Pt-100), whose accuracy was within 0.05°C . The pressure drop was calculated from the static and dynamic pressures detected by the pitot tube. All the data signals were collected and converted by a data acquisition system.

The estimated uncertainty is 3% for the mean temperature and 7.1% for the pressure drop. Using the method proposed by Kline and McClintock,⁽¹⁷⁾ the maximum uncertainty of the calculated local convective heat transfer coefficient is $\pm 7.8\%$.

3. RESULTS AND DISCUSSION

The numerical results for the bare tube (inside diameter of the tube = 0.042 m), flat plane inserts ($\delta = 0.0016$ m), flat plane inserts with holes, and the twisted-tape inserts with different twisted angles ($\alpha = 15.3^\circ$, 24.4° and 34.3°) are shown in Figs 4~6. Figure 4 illustrates the velocity distribution for the circular tube with flat plane inserts, flat plane inserts with holes, and twisted-tape inserts with an inlet frontal velocity 9.5 m/s.

For the flat plane inserts and flat plane inserts with holes, Figs. 4(a) and 4(b) show that the velocity along the central line are much higher than that of the bare tube. Furthermore, as shown in Fig. 4(a), the boundary layer is repeatedly interrupted by the holes on the flat plane inserts and results in the flow re-mixing near the holes. The velocity distributions of three types of the twisted-tape tube inserts are shown in Figs. 4(c), 4(d) and 4(e). The flow inside the tubes was mixed by the twisted-tape inserts and was accelerated to a value 40% higher than the inlet velocity due to the distortion of the flow field.

The numerical results of pressure distribution for a circular tube with inserts with an inlet velocity 9.5 m/s is presented as Fig. 5. As shown in Fig. 5(a), the working fluid flows pass-by the flat plane and results in a great pressure drop due to the resistance on the surface of the inserts. Comparing Figs. 5(a) and 5(b), it is clear that the pressure drop for the flat plane inserts is about 50% higher than that for the flat plane with holes due to the destruction of the boundary layer near the flat plane. Figures 5(c), 5(d) and 5(e) show the pressure distribution of the working fluid in a circular tube with twisted-tape inserts. The pressure drop for the insert

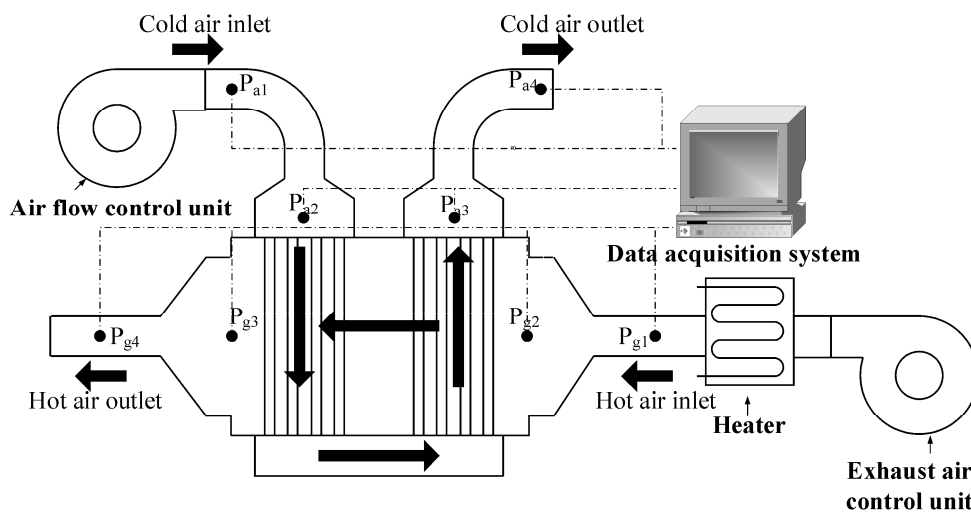


Fig. 3. Schematic diagram of the experimental setup.

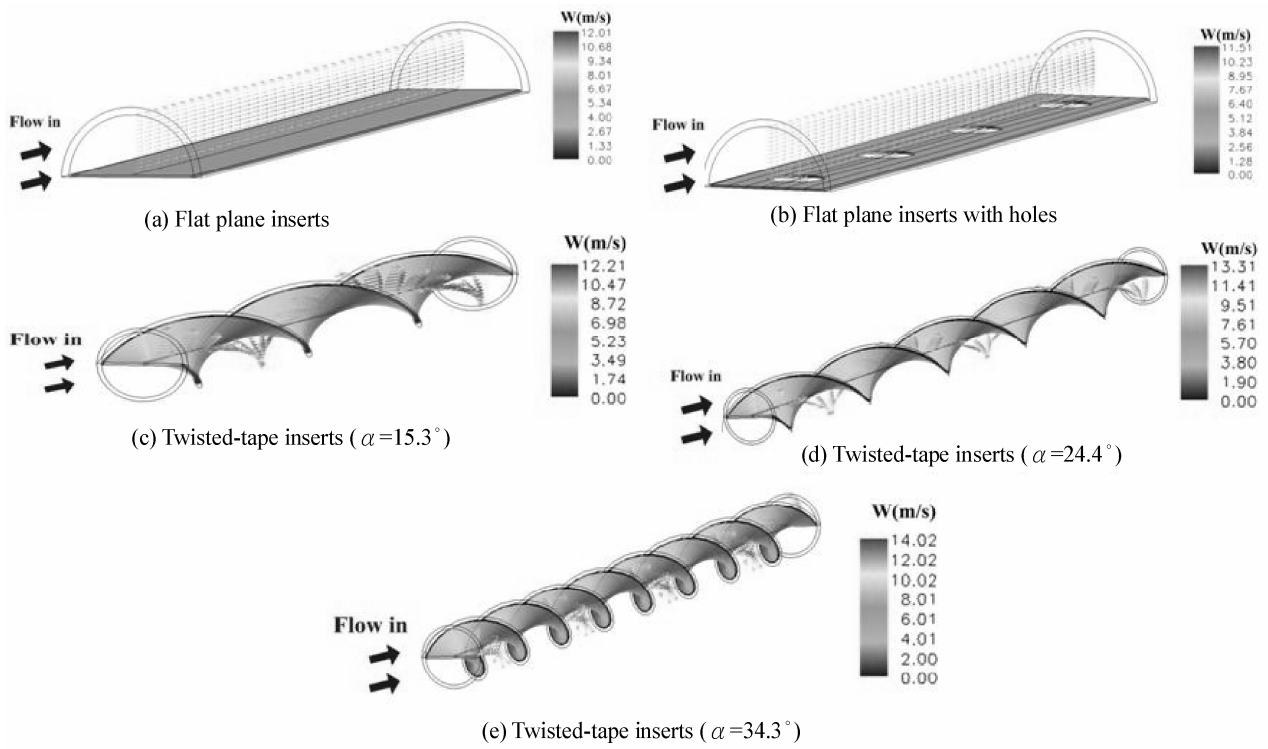


Fig. 4. Velocity distribution inside the tube with tube inserts.

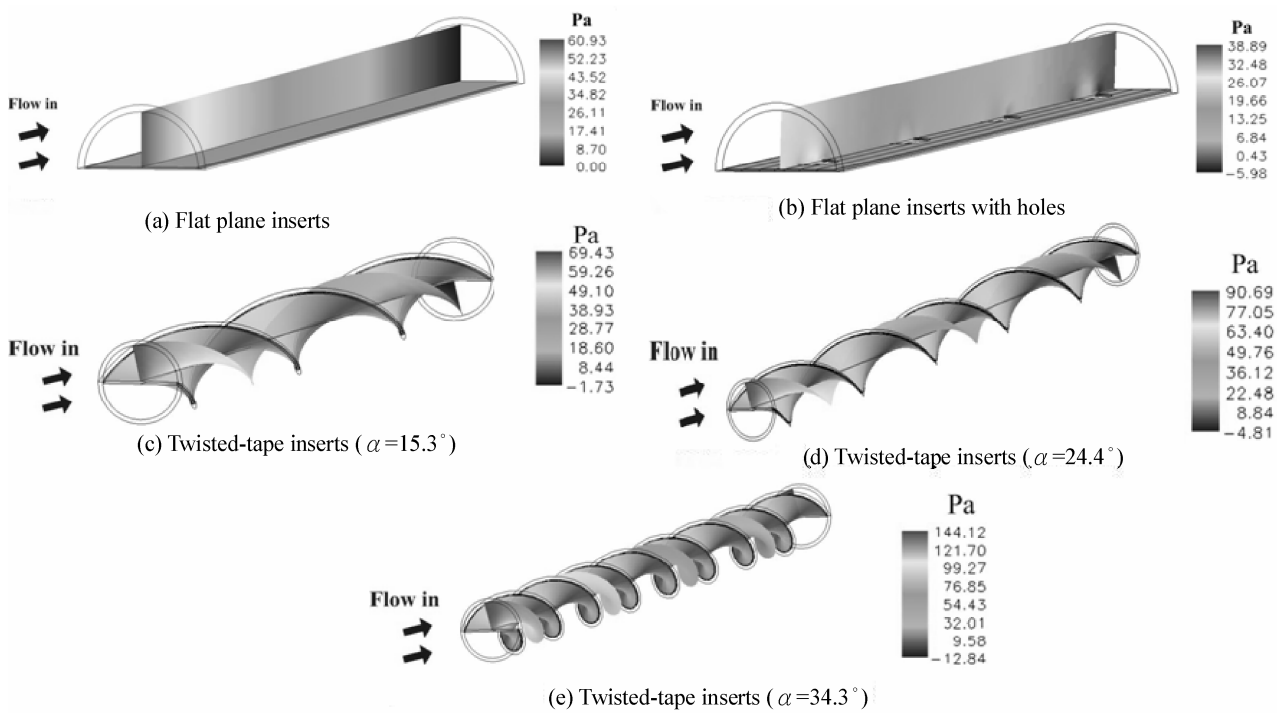


Fig. 5. Pressure distribution inside the tube with tube inserts.

with $\alpha = 34.3^\circ$ is 109% higher than that for the insert with $\alpha = 15.3^\circ$ and 59% higher than that for the insert with $\alpha = 24.4^\circ$.

The temperature distributions for a cross section

for different tube inserts are presented in Fig. 6, 6(a) and 6(b) show the temperature distribution for a cross section in a circular tube with flat plane inserts with and without holes. It is seen that the low tempera-

ture region for a flat plane insert with holes is larger than that for a bare flat plane insert due to the heat transfer enhancement by the holes on the flat plane insert. The temperature distributions of a circular tube with the twisted-tape inserts are presented in Figs. 6(c), 6(d) and 6(e). A cross section of the twisted tube for temperature field was selected and the temperature distributions are presented in two dimensional forms in these figures.

Figure 7 demonstrates the pressure drop per unit length in a circular tube with different kinds of tube inserts versus Reynolds number Re_{Dh} . It is seen from Fig. 7 that the highest pressure drop occurred when the twisted-tape insert type C with twist angle 34.3° was used. Significantly, the pressure drop in a circular tube with twisted-tape inserts was about 45~102% larger than that with flat plane inserts. It is also observed that for the flat plane tube insert with holes, the pressure drop was about 5~38% higher than that for twisted-tape inserts type A with twist angle 15.3° , since boundary layer destruction occurs due to the holes in the flat plane inserts.

The numerical results and the experimental data of the mean Nusselt numbers obtained for the bare tube, the tube with flat-plane insert, the tube with flat plane

insert with holes, and the tube with twisted tape insert type B with twist angle 24.4° are shown in Fig. 8. It is seen that the heat transfer performance of the twisted-tape tube insert type B, with twist angle 24.4° , is the best one among all test cases in this study. The mean Nusselt number for the twisted-tape inserts with twist angle 24.4° is 6~18% higher than that for flat plane inserts with holes, 12~27% higher than that of flat plane inserts and 22~35% higher than the bare tube.

In Fig. 9, the mean Nusselt number data with different twist angles ($\alpha = 15.3^\circ, 24.4^\circ$ and 34.3°) are compared. The results of the heat transfer performance from the correlation predicted by Thorsen and Landis,⁽¹²⁾ Donevski et al.⁽¹⁸⁾ and Kidd⁽¹⁹⁾ are also graphically presented and compared in Fig. 9 on the basis of the following: $y = 2.5, \delta/d_i = 0.05, L/d_i = 150$. It is seen that there is a fair agreement between the results reported by Thorsen & Landis and Donevski *et al.* and the correlation obtained by Kidd was a little over-predicted. It can be seen from Fig. 9 that the correlation obtained in this study predicts the mean Nusselt number as well as that for correlations of other investigators within 20%.

Figure 10 presents the variations of the Colburn factor (j) and the friction factor (f) with the Reynolds number Re_{Dh} for the bare tube, the tubes with flat-plane

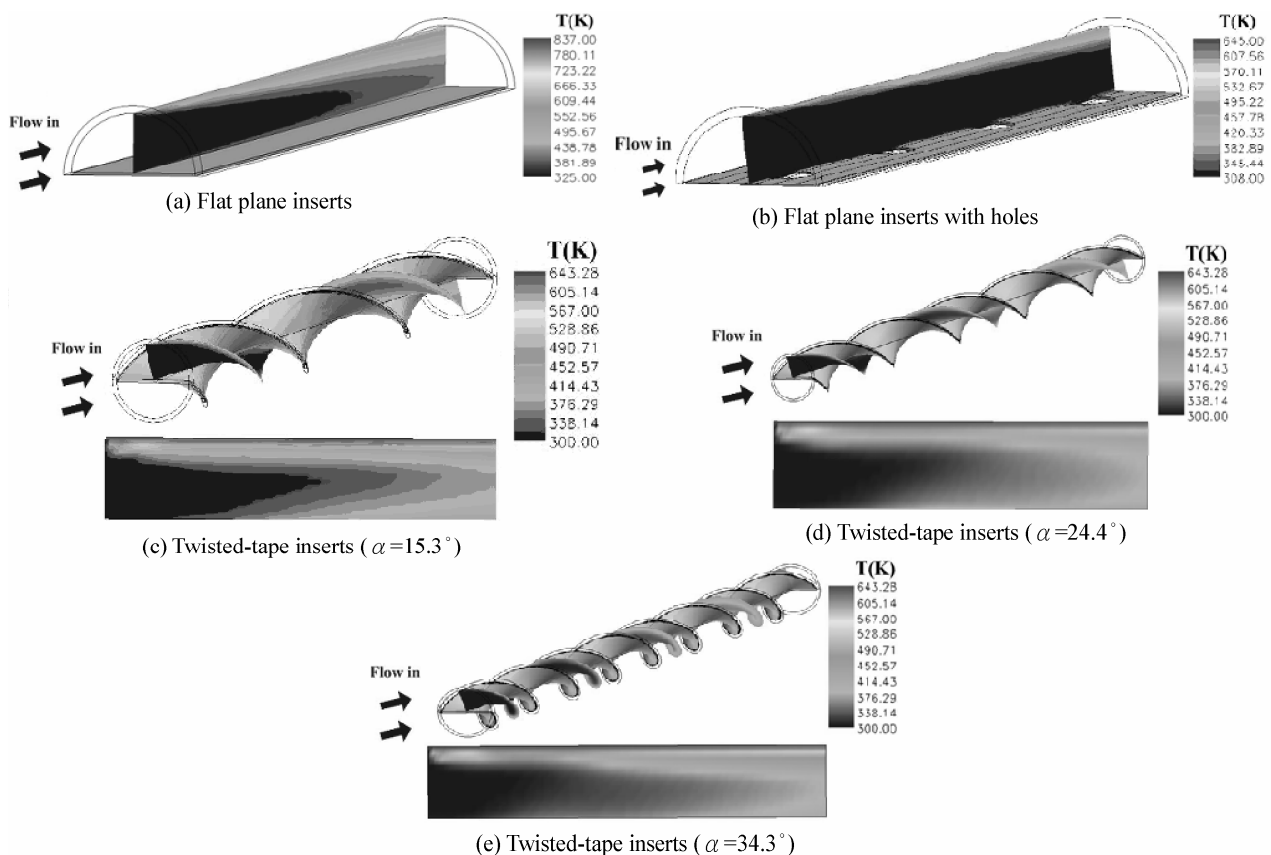


Fig. 6. Temperature distribution inside the tube with tube inserts.

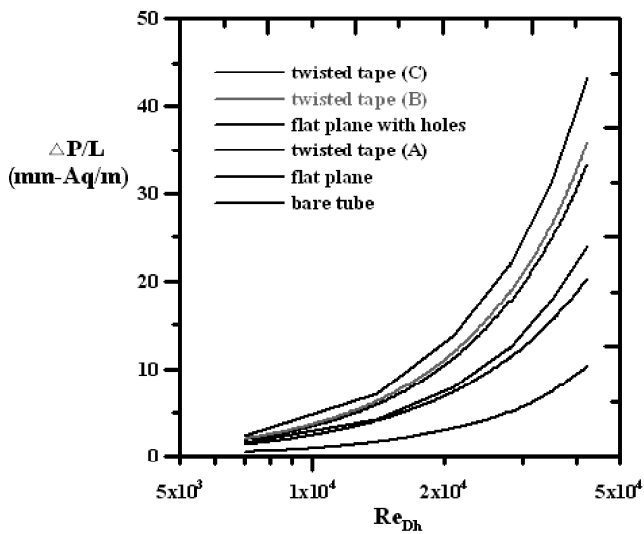


Fig. 7. Pressure drop per unit length of tube for different kind of tube inserts.

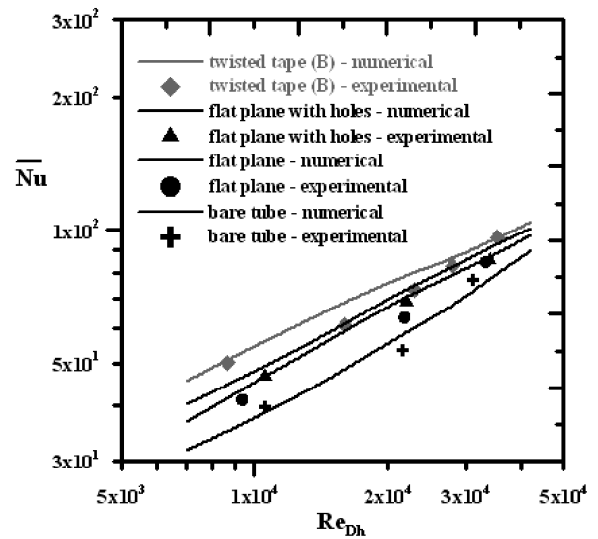


Fig. 8. Nusselt number for different kind of tube inserts.

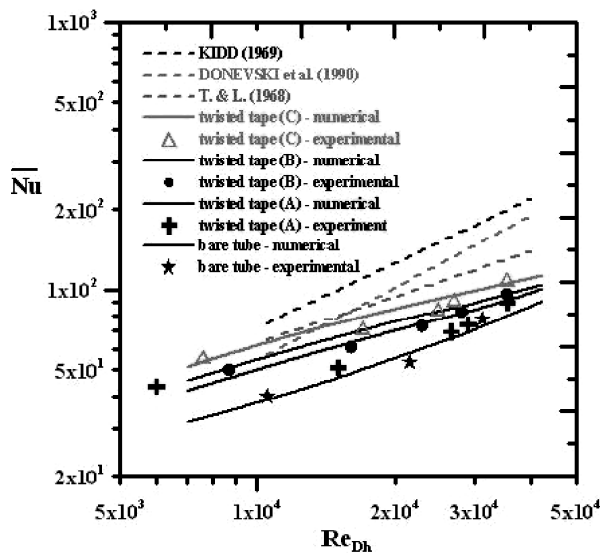


Fig. 9. Nusselt number for twisted inserts with different twist angles.

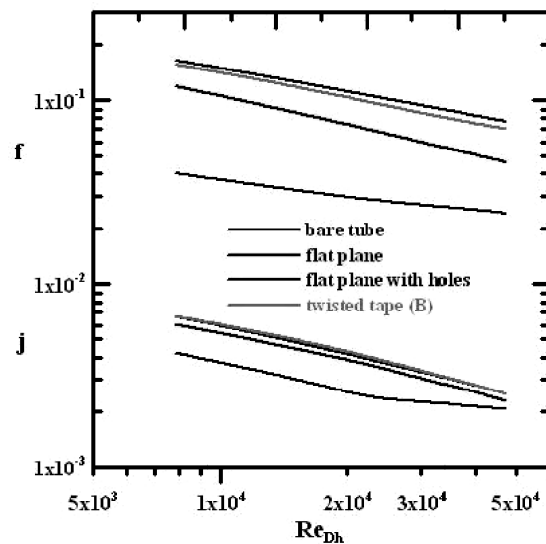


Fig. 10. Heat transfer and friction factor for various inserts.

inserts, flat-plane inserts with holes, and the twisted-tape inserts type B, with twist angle 24.4° , respectively. Although the Colburn factor (j) of the twisted-tape inserts is only 2~5% higher than that of the flat plane inserts with holes, the friction factor (f) of the twisted-tape inserts is 3~8% lower than that of the flat plane inserts with holes. As a result, the twisted-tape tube inserts with twist angle 24.4° are more suitable and economical for industry applications.

Finally the correlations obtained from numerical method for the Nusselt number (Nu) and friction factor (f) are shown in Table 1.

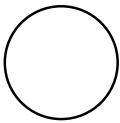
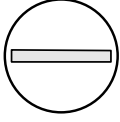
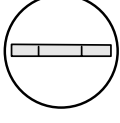
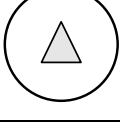
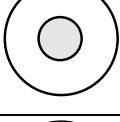
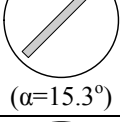
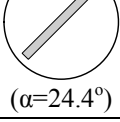
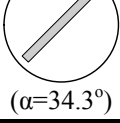
4. CONCLUSIONS

The numerical and experimental studies of three-dimensional turbulent flow inside the tubes with flat plane inserts, flat plane inserts with holes and twisted-tape inserts with three different twist angles ($\alpha = 15.3^\circ, 24.4^\circ$ and 34.3°) have been presented. Heat transfer performance and related pressure drop were also discussed in this study. The numerical results demonstrate that the average heat transfer coefficient of tubes with twisted-tape inserts are 6~35% higher than that for flat plane inserts with holes according to the different

twist angles from 15.4° to 34.3° . The numerical predictions agree well with the experimental results and with the data presented in the literature. The influence of the different types of tube insert in a circular tube may be summarized as follows:

- (1) The flat plane inserts with holes in a circular tube have the greater enhancement of the heat transfer coefficient than that for a flat plane insert and result in a higher pressure drop and a larger friction factor.
- (2) A higher twist angle of the twisted-tape inserts induces a larger heat transfer coefficient, but give rise to a flow penalty in the form of an increased friction factor.
- (3) The heat transfer coefficient for a circular tube with flat plane inserts with holes is greater than that for a twisted-tape insert type A, with $\alpha = 15.4^\circ$, and worse than that for a twisted-tape insert type B, where $\alpha = 24.3^\circ$.

Table 1 Correlations of Mean Nusselt Number and Friction Factor

		C_1	m_1	C_2	m_2
	$7000 \leq Re \leq 20000$	0.02209	0.7673	0.7594	-0.3274
	$20000 \leq Re \leq 50000$	0.01809	0.7875	0.2743	-0.2246
	$7000 \leq Re \leq 20000$	0.1889	0.5824	11.1752	-0.5065
	$20000 \leq Re \leq 50000$	0.5025	0.4836	16.195	-0.544
	$7000 \leq Re \leq 20000$	0.2291	0.5679	6.647	-0.4125
	$20000 \leq Re \leq 50000$	0.6577	0.4614	8.3624	-0.4356
	$7000 \leq Re \leq 20000$	0.04318	0.7159	0.5965	-0.2097
	$20000 \leq Re \leq 50000$	0.02432	0.7739	0.5369	-0.1991
	$7000 \leq Re \leq 20000$	0.03132	0.7496	0.9108	-0.1989
	$20000 \leq Re \leq 50000$	0.0293	0.7563	0.6504	-0.1646
 ($\alpha=15.3^\circ$)	$7000 \leq Re \leq 20000$	0.5746	0.4745	1.5301	-0.3042
	$20000 \leq Re \leq 50000$	0.8845	0.4317	2.673	-0.3617
 ($\alpha=24.4^\circ$)	$7000 \leq Re \leq 20000$	0.7685	0.4531	2.3676	-0.3245
	$20000 \leq Re \leq 50000$	1.546	0.3837	2.949	-0.348
 ($\alpha=34.3^\circ$)	$7000 \leq Re \leq 20000$	1.2035	0.4191	2.6511	-0.3166
	$20000 \leq Re \leq 50000$	1.663	0.387	3.019	-0.3281

$$\overline{Nu} = C_1 Re^{m_1} ; f = C_2 Re^{m_2}$$

NOMENCLATURE

A	Heat transfer area of tube inserts (mm^2)
d	Diameter of the tube (mm)
d_o	Outside diameter of the tube (mm)
d_i	Inside diameter of the tube (mm)
C	Heat capacity (W/kg-K)
D_h	Hydraulic diameter (mm)
f	Friction factor
Gr	Grashof number
H	Width of the tube inserts (mm)
h	Heat transfer coefficient ($\text{W/m}^2\text{-K}$)
\bar{h}	Average heat transfer coefficient ($\text{W/m}^2\text{-K}$)
j	Colburn factor
$j_{bare\ tube}$	Colburn factor of the bare tube
K	Thermal conductivity (W/m-K)
L	Axial length (m)
Nu	Nusselt number
Nu_d	Nusselt number of the tube with twisted-tape inserts
$Nu_{d,y=\infty}$	Nusselt number of the tube with flat-plane inserts
\bar{Nu}	Average Nusselt number
U_{in}	Inlet velocity
P	Pressure (Pa)
P_{in}	Inlet pressure (Pa)
P_t	The length of the twisted-tape twist from 0° to 180° (mm)
P_{total}	Total pressure drop (mm-Aq)
Pr	Prandtl number
Q	Heat transfer rate (W)
q or q''	Heat flux (W/m^2)
Re	Reynolds number
Re_d	Reynolds number based on d
Re_{Dh}	Reynolds number based on D_h
St	Stanton number
T	Temperature (K)
δ	Thickness of the tube inserts (mm)
T_{in}	Inlet temperature (K)
T_w	Wall temperature (K)
t_w	Tube wall thickness (mm)
u,v,w	Flow velocity along x,y,z axis (m/s)
y	Twist ratio
α	Twist angle

REFERENCES

1. R. Koch: Druckverlust und Waermeuebergang bei Verwirbeiter, Verein Deutscher Ingenieure Forschungsheft. Series B (1958) 24, No. 469, pp. 1-44.
2. L. B. Evans and S. W. Churchill: The Effect of Axial Promoters on Heat Transfer and Pressure Drop inside a Tube, Chemical Engineering Progress Symposium Series 59 (1963) 41, pp. 36-46.
3. D. G. Thomas: Enhancement of Forced Convection Mass Transfer Coefficient Using Detached Turbulence Promoters, Industrial Engineering and Chemical Process Design Developments (1967) 6, pp. 385-390.
4. L. Xie, R. Gu and X. Zhang: A study of Optimum Inserts for Enhancing Convective Heat Transfer of High Viscosity Fluid in a Tube, Multiphase Flow and Heat Transfer, Second International Symposium (1992) 1, X-J. Chen T. N., Veziroglu and C. L. Tien Eds., Hemisphere Publishing Corp., New York, pp. 649-656.
5. W. H. Emerson: Heat Transfer in a Duct in Regions of Separated Flow, Proceedings of the Third International Heat Transfer Conference (1961) 1, pp. 267-275.
6. W. E. Hilding and C. H. Coogan: Heat Transfer and Pressure Drop in Internally Finned tubes, ASME Symposium on Air Cooled Heat Exchangers (1964), pp. 57-84.
7. A. C. Trupp and A. C. Y. Lau: Fully Developed Laminar Heat Transfer in Circular Sector Ducts with Isothermal Walls", Journal of Heat Transfer (1984) 106, pp. 467-469.
8. A. W. Date and J. R. Singham: Numerical Prediction of Friction and Heat Transfer Characteristics of Fully Developed Laminar Flow in Tubes Containing Twisted Tapes, ASME paper 72-HT-17 (1972).
9. A. W. Date: Prediction of Fully Developed Flow in a Tube Containing a Twisted Tape, International Journal of Heat and Mass Transfer (1974) 17, pp. 845- 859.
10. W. J. Marner and A. E. Bergles: Augmentation of Highly Viscous Laminar Tube-side Heat Transfer by Means of a Twisted-Tape Insert and an Internally Finned Tube, Advances in Enhanced Heat Transfer, ASME Symposium, HTD (1985) 43, pp. 19-28.
11. R. Smithberg and F. Landis: Friction and Forced Convection Heat Transfer Characteristics in Tubes with Twisted Tape Swirl Generators", Journal of Heat Transfer (1964) 87, pp. 39-49.
12. R. Thorsen and F. Landis: Friction and Heat Transfer Characteristics in Turbulent Swirl Flow Subjected to Large Transverse Temperature Gradients, Journal of Heat Transfer (1968) 90, pp. 87-89.
13. R. F. Lopina and A. E. Bergles: Heat Transfer and Pressure Drop in Tape-Generated Swirl Flow of Single-Phase Water, Journal of Heat Transfer (1969) 91, pp. 434-442.
14. R. M. Manglik and A. E. Bergles: Heat Transfer and Pressure Drop Correlations for Twisted-Tape Inserts in Isothermal Tubes: Part I-Laminar Flows in ASME Symposium on Enhanced Heat Transfer Edited by Pate M. B. and Jensen M. K., HTD (1992)

- 202, pp. 89-98.
15. T. S. Wang and Y. S. Chen: Unified Navier-Stokes Flow Field and Performance Analysis of Liquid Rocket Engines, *AIAA Journal* (1993) 9 (5), pp. 678- 685.
 16. W. A. Fiveland: Three Dimensional Radiative Heat- Transfer Solutions by the Discrete Ordinates Method, *Journal of Thermophysics and Heat Transfer* (1988) 2.4, pp. 309-316.
 17. S. J. Kline and F. A. McClintock: Describing Uncertainties Single-Sample Experiment, *ASME Mechanical Engineering* (1953) 75, pp. 3-8.
 18. B. Donevski and J. Kulesza: Resistance Coefficients for Laminar and Turbulent Flow in Swirling Ducts, *Archiwum Termodynamiki I Spalania* (1978) 9, No. 3, pp. 497-506, (in Polish).
 19. G. J. Kidd Jr.: Heat Transfer and Pressure Drop for Nitrogen Flowing in Tubes Containing Twisted Tapes, *AIChE Journal* (1969) 15, pp. 581-585. □